JOURNAL OF SYNCHROTRON RADIATION
ISSN 1600-5775

Phenomenological and numerical analysis of power evolution and bunching in single-pass X-ray FELs. Erratum

K. Zhukovsky* and A. Kalitenko

Department of Theoretical Physics, Faculty of Physics, M. V. Lomonosov Moscow State University, Moscow 119991, Russian Federation. *Correspondence e-mail: zhukovsk@physics.msu.ru

Received 8 December 2018
Accepted 4 February 2019

Edited by M. Yamamoto, RIKEN SPring-8 Center, Japan

Keywords: undulator radiation; two-frequency undulator; harmonic generation; free-electron laser.

A correction is made to the paper by Zhukovsky & Kalitenko (2019). [*J. Synchrotron Rad.* **26**, 159–169].

In our previous work (Zhukovsky & Kalitenko, 2019) we modelled and commented on an LCLS experiment, stating that the third harmonic was not registered in it. We followed Emma *et al.* (2010) and realised that we were mistaken. Indeed, a later study of the third and second harmonics in this experiment was reported by Ratner *et al.* (2011). The radiation of the third harmonic was registered in the hard X-ray LCLS experiment.

Our phenomenological modelling of the harmonic power of 1.5 Å free-electron laser (FEL) radiation in the LCLS experiment for $\gamma = 26600$, $\sigma_\varepsilon = 1 \times 10^{-4}$, $\varepsilon_{x,y} = 0.4$ µm rad, $\lambda_u = 3$ cm, $k = 3.5$ was presented in Fig. 5 of Zhukovsky & Kalitenko (2019). Now we add to it the comparison with the experimentally measured data from Ratner *et al.* (2011) and Emma *et al.* (2010). The fundamental harmonic measurements correspond to the coloured dots, following the data of Emma *et al.* (2010). The experimentally allowed range for the third harmonic is denoted by the shadowed area, following the data of Ratner *et al.* (2011). The third harmonic in our phenomenological simulation — the green line — fits in the middle of the range [see Fig. 1 below, which complements Fig. 5 in our earlier work (Zhukovsky & Kalitenko, 2019)].

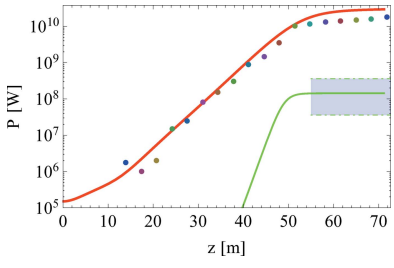

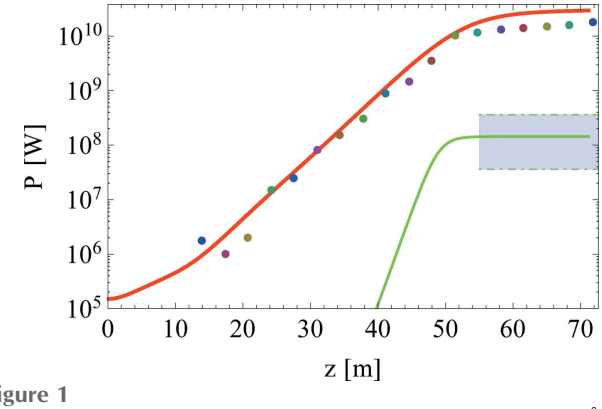

Figure 1
Phenomenological modelling of the harmonic power in the 1.5 Å FEL radiation LCLS experiment for $\gamma = 26600$, $\sigma_\varepsilon = 1 \times 10^{-4}$, $\varepsilon_{x,y} = 0.4$ µm rad, $\lambda_u = 3$ cm, $k = 3.5$. Harmonics in the phenomenological model (solid lines): $n = 1$, red; $n = 3$, green. The shadowed area denotes the range of experimental values for the third harmonics, reported by Ratner *et al.* (2011).

A perfect fit of the predicted values in the experimentally measured range further confirms the validity of our approach and modelling. Some higher than measured saturated power for the fundamental tone is explained by the fact that the phenomenological model gives the peak power for the fundamental tone and does not reproduce its oscillations in the saturated regime. The second harmonic was not registered in the hard X-ray band; it was registered only in the soft X-ray band and was ∼20–50 times weaker than the third harmonic: 0.04–0.1% of the fundamental tone power (Ratner *et al.*, 2011). The saturated power of the second harmonic, estimated in the framework of the phenomenological approach, appeared lower than the initial power of the fundamental tone. Thus it is not present in Fig. 1; it also agrees with the results of Ratner *et al.* (2011).

We apologize for the misprinted formula (14) in the original paper (Zhukovsky & Kalitenko, 2019). The correct version follows:

$$
\begin{aligned}
f_{n,x} &= I^{(h)}_{n-1}(n) + I^{(h)}_{n+1}(n) + (d/h)\left[I^{(h)}_{n+h}(n) + I^{(h)}_{n-h}(n)\right],\\
I^{(h)}_{n}(m) &= \int_0^{2\pi} \frac{d\varphi}{2\pi}\cos\left[n\varphi + \frac{mk^2(\xi_1+\xi_2+\xi_3+\xi_4)}{1+k^2_{\rm eff}/2}\right],\\
\xi_1 &= \frac{\sin(2\varphi)}{4}, \qquad \xi_2 = \frac{d\sin[(h-1)\varphi]}{h(h-1)},\\
\xi_3 &= \frac{d\sin[(h+1)\varphi]}{h(h+1)}, \qquad \xi_4 = \frac{d^2\sin(2h\varphi)}{4h^3}.
\end{aligned}
\tag{14}
$$

Further study will be presented in a dedicated forthcoming publication.

References

Emma, P. *et al.* (2010). *Nat. Photon.* **4**, 641–647.

Ratner, D., Brachmann, A., Decker, F. J., Ding, Y., Dowell, D., Emma, P., Fisher, A., Frisch, J., Gilevich, S., Huang, Z., Hering, P., Iverson, R., Krzywinski, J., Loos, H., Messerschmidt, M., Nuhn, H. D., Smith, T., Turner, J., Welch, J., White, W. & Wu, J. (2011). *Phys. Rev. ST Accel. Beams*, **14**, 060701.

Zhukovsky, K. & Kalitenko, A. (2019). *J. Synchrotron Rad.* **26**, 159–169.

JOURNAL OF SYNCHROTRON RADIATION

ISSN 1600-5775

Phenomenological and numerical analysis of power evolution and bunching in single-pass X-ray FELs

K. Zhukovsky* and A. Kalitenko

Department of Theoretical Physics, Faculty of Physics, M. V. Lomonosov Moscow State University, Moscow 119991, Russian Federation. *Correspondence e-mail: zhukovsk@physics.msu.ru

Received 9 March 2018
Accepted 4 September 2018

Edited by M. Yamamoto, RIKEN SPring-8 Center, Japan

Keywords: undulator radiation; two-frequency undulator; harmonic generation; free-electron laser.

The harmonic power and bunching evolution in X-ray single-pass free-electron lasers (FELs) is modelled and the harmonic generation in a phase-shifted two-frequency FEL is explored. The advanced phenomenological FEL model, which is validated numerically and experimentally, is employed. The model accounts for major losses for each harmonic individually; it is compared with reported experimental data and with *PERSEO* numerical simulations, which are performed here for a variety of experiments. The latter cover the radiation wavelength range 0.15–300 nm. The phenomenological description is based on a few key FEL parameters: electron beam section, current, energy and its spread and divergence. The model is employed for modelling harmonic bunching and power evolution in a phase-shifted X-ray FEL with a two-frequency undulator, where lower harmonics with numbers less than nth are suppressed by the electron–photon phase shift of $k\pi/n$, $k = 2, 4, \ldots$, between the undulator sections. The benefits of the two-frequency phase-shifted FEL are highlighted. FEL-induced energy spread is shown to be three times lower than in a FEL without the phase-shift. The high-power harmonic and sub-harmonic radiation in such a FEL is demonstrated. In particular, powerful $\sim$14 GW X-ray radiation at $\lambda_5 = 0.15$ nm from electrons with energy of 5.47 GeV and beam current $\sim$3.66 kA is possible in a two-frequency phase-shifted FEL at 30 m; this constitutes half of a FEL length where a common planar undulator radiates the same wavelength and power at the fundamental harmonic. Moreover, about a three times lower energy spread is induced by the dominant fifth harmonic, and the harmonic power can be thousands of times higher than in a common planar undulator FEL.

1. Introduction

First sources of coherent radiation, *i.e.* lasers, appeared in the 1960s and worked in the infrared region. Since then, significant efforts have been made to develop higher-frequency sources of coherent radiation and reach the X-band, where synchrotron radiation has been the strongest source for a long time. However, the conventional approach, which is based on population inversion in the laser's body, does not extend to X-rays; the bottom limit for a common laser wavelength is $\sim$100 nm. Synchrotron and undulator radiation (UR) both originate from relativistic charges with significant Lorentz factors $\gamma = 1/[1 - (v/c)^2]^{1/2} \gg 1$, where v is the charge velocity and c is the speed of light; then $\gamma \cong E/mc^2 \gg 1$, where E is the electron rest energy and m is its mass. Synchrotron radiation and UR can have high power in the X-ray band, though both are incoherent.

The idea of an undulator device where charges perform small transversal oscillations in a spatially periodic magnetic field and drift at relativistic speeds along the undulator axis was proposed by Ginzburg (1947). He also proposed that this

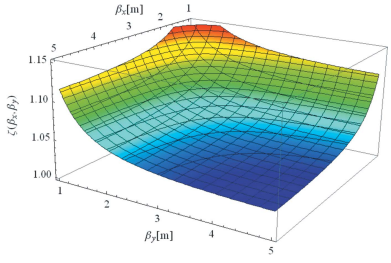

radiation can be coherent if it comes from a series of electron bunches, separated by the radiation wavelength, where the length of the bunch is shorter than the UR wavelength. The first undulator was built and tested by H. Motz in 1951 (Motz *et al.*, 1953). Nowadays, UR is the focus of research in the context of free-electron lasers (FELs). In these devices the radiation interacts with macro-bunches of electrons in undulators. It groups electrons in micro-bunches at every radiation wavelength period and thus coherent UR is formed towards the end of the undulator; the radiation intensity exponentially grows along the FEL-undulator length.

FELs are capable of generating coherent X-rays with peak power exceeding that of synchrotron radiation in the X-ray band (McNeil & Thompson, 2010; Pellegrini *et al.*, 2016; Huang & Kim, 2007; Saldin *et al.*, 2000, 2010; Bonifacio *et al.*, 1984; Schmüser *et al.*, 2014; Pellegrini, 2016; Margaritondo & Ribic, 2011; Margaritondo, 2017, 2015; Bagrov *et al.*, 2002; Seddon *et al.*, 2017). It has multiple applications for imaging and in medicine *etc.* (see, for example, Albertin *et al.*, 2015; Frank *et al.*, 2014). In a multi-pass FEL the radiation is confined to an optical cavity with reflecting semi-transparent mirrors, just like in a common laser. This construction benefits from the modes of the optical elements, which helps set the radiation structure, but the mirror's material imposes frequency limitations in the X-ray band where rare reflectivity peaks can be found (Bajt & Wall, 2000, 2002). Beyond the low-gain regime, the high-gain FEL (Bonifacio *et al.*, 1984; Kroll & McMullin, 1978; Colson, 1997; Sprangle & Smith, 1980; Kim & Xie, 1993) regime exists. In such FELs the radiation passes through a long undulator once. This single-pass design does not require optical resonators, whose reflectivity limits the FEL frequency. In a single-pass self-amplified spontaneous-emission (SASE) FEL the generation begins with the initial noise; a weak coherent seed can be added for better phase stability. The output of a SASE FEL constitutes a train of pulses which has good spatial structure, but poor temporal coherence due to random initial noise. Seeding in the X-ray band is difficult. An alternative solution is the generation and amplification of high FEL harmonics of a low seed frequency as proposed by Yu *et al.* (2000), Yu (1991), Saldin *et al.* (2002), Shaftan & Yu (2005), Li & Jia (2013), Deng & Dai (2010, 2013) and Zeng *et al.* (2016) and realized by Shintake (2008), Yu *et al.* (2003), McNeil (2008) and Tiedtke *et al.* (2009). Two-frequency undulators were shown (Zhukovsky, 2014, 2015*a*,*b*, 2016*a*; Mishra *et al.*, 2009) to generate FEL harmonics with high power (Dattoli *et al.*, 2006, 2014) in a linear regime; bunching coefficients for the harmonics in two-frequency undulators also exceed by far the respective values in common planar undulators (Zhukovsky & Potapov, 2017). Thus two-frequency undulators were proposed for prebunchers in cascaded FELs (Zhukovsky, 2017*a*,*b*,*c*, 2018*a*,*b*,*c*). High-gain FELs are usually simulated with one-dimensional or three-dimensional numerical models based on solutions to sets of equations for many electrons in the field of the wave and its harmonics. The beam geometry, focusing, Twiss parameters *etc.* (Quattromini *et al.*, 2012; Walker, 1993; Vinokurov & Levichev, 2015; Onuki & Elleaume, 2003) are all accounted for. However, the use of these complicated numerical codes requires knowledge of all the particularities of the installation, trained personnel and adequate computing resources.

Our phenomenological model accounts individually for the losses of each harmonic with the number n in undulator sections different from each other. Now the model also includes the coupling losses between the cascades. Different from previous versions (see Zhukovsky & Potapov, 2017; Zhukovsky, 2017*a*,*b*,*c*, 2018*a*,*b*,*c*), in the following we account for asymmetric electron beams and coupling losses between undulator cascades. Moreover, we include in the phenomenological model the description of the case when lower harmonics are suppressed by displacing electrons to the photon pulse between the undulator sections.

In the following we will demonstrate that, for a preliminary analysis of a FEL operation, close to experimental results for the FEL harmonic power and bunching can be achieved with a phenomenological description that is much simpler than 3D simulations. The phenomenological model can be easily implemented in any mathematical program on any PC, and basic evaluations can be made even on a calculator with elementary formulae. The results are compared with experiments and with 1D simulations as well.

Moreover, we will demonstrate that it is possible to make a dominant fifth harmonic in a $\sim$30 m FEL with a two-frequency undulator, and achieve $\sim$13 GW power at $\lambda \simeq$ 0.15 nm wavelength with $\sim$3.7 kA current and $E \simeq 5.47$ GeV electron energy.

2. Phenomenological description of an ideal single-pass FEL

A basic semi-analytical description of radiation power evolution along a single-pass FEL was developed by G. Dattoli on the basis of a logistic equation (Dattoli, 1998). The nth harmonic power exponentially grows along the axial z-coordinate from the initial power $P_{0,n}$ to the saturated power $P_{n,F} = (P_F/\sqrt{n})(f_n/nf_1)^2$, limited by the saturation of the fundamental harmonic at

$$P_F \cong \sqrt{2}\rho_1 P_{\rm e},$$

where

$$\rho_n = \frac{1}{2\gamma}\left[\frac{J}{4\pi i}\left(\lambda_{\rm u}\, k_{\rm eff}\, f_n\right)^2\right]^{1/3}$$

is the Pierce parameter, fundamental in FEL physics (see, for example, Saldin *et al.*, 2000; Bonifacio *et al.*, 1984), $P_{\rm e}$ is the electron beam power, $\lambda_{\rm u}$ is the main undulator period [m], $k_{\rm eff}$ is the effective undulator parameter (Zhukovsky, 2016*a*), which for a common undulator reads

$$k = \frac{e}{mc^2}\frac{H_0\lambda_{\rm u}}{2\pi} \simeq H_0\lambda_{\rm u}\ [{\rm T\,cm}],$$

H_0 is the strength of the magnetic field on the axis, f_n are the Bessel coefficients for the UR harmonic n (see, for example, Dattoli *et al.*, 2006, 2014), which for a common undulator reads

$$f_{n,x} = J_{(n-1)/2}(n\xi) - J_{(n+1)/2}(n\xi)$$

in terms of common Bessel functions $J_n(\xi)$, $\xi = k^2/4(1 + k^2/2)$, J is the electron current density [A m^{-2}], and $J \cong 1.7045 \times 10^4$ is the Alfven current [A]. The initial power is provided by the seed or by minor coherent fluctuations in the initial shot noise in a SASE FEL; for an unbunched electron beam only $\sim$1/9 of the initial radiation power couples to electrons for bunching (McNeil & Thompson, 2010; Pellegrini *et al.*, 2016; Huang & Kim, 2007; Saldin *et al.*, 2000; Bonifacio *et al.*, 1984; Schmüser *et al.*, 2014). The power growth along z is approximated by the following logistic function (Dattoli *et al.*, 2006; Dattoli & Ottaviani, 2002),

$$P_{L,n}(z) \cong \frac{P_{0,n}A(n,z)\,\exp(0.223z/Z_s)}{1 + [A(n,z) - 1]\left(P_{0,n}/P_{n,F}\right)} \tag{1}$$

$$A(n,z) \cong \frac{1}{3} + \frac{\cosh(z/L_{n,g})}{4.5} + \frac{\cos(\sqrt{3}z/2L_{n,g})\cosh(z/2L_{n,g})}{0.444}$$

where $L_{n,g} \cong \lambda_u/(4\pi\sqrt{3}n^{1/3}\rho_n)$ is the gain length for the nth FEL harmonic, and $Z_s \cong 1.07L_{1,g}\ln(9P_F/P_{0,1})$ is its saturation length. In a prebunched beam the harmonic radiation power evolves along z according to another logistic function (Dattoli *et al.*, 2005),

$$P_{L,n}(z) \cong \frac{P_{0,n}F(n,z)}{1 + F(n,z)\left(P_{0,n}/P_{n,F}\right)}, \tag{2}$$

$$F(n,z) \cong \left|2\left(\cosh\frac{z}{L_{n,g}} - \cos\frac{z}{2L_{n,g}}\cosh\frac{z}{2L_{n,g}}\right)\right|,$$

where $P_{0,n}$ is the initial power of the harmonic n, which comes directly from the previous FEL section or is provided by the bunching. The continuity of the latter is ensured by the renormalization factor $\rho_{1,\mathrm{sec}\,1}/\rho_{1,\mathrm{sec}\,2}$ for undulators different from each other in neighbouring cascades. The above formulae (1)–(2) describe independent linear harmonic generation, which is complemented by the non-linear term, induced by the dominant fundamental harmonic. In a non-linear regime the nth harmonic power grows faster, as the nth power of the dominant fundamental harmonic (Dattoli *et al.*, 2005; De Martini, 1990; Bonifacio *et al.*, 1990; Huang & Kim, 2000),

$$Q_n(z) \cong P_{n,0}\,\frac{\exp\left(nz/L_g\right)}{1 + \left[\exp\left(nz/L_g\right) - 1\right]P_{n,0}/P_{n,F}}, \tag{3}$$

where $L_g \equiv L_{1,g}$, $P_{n,0} \cong d_n b_n^2 P_{n,F}$ is the equivalent power due to the bunching, $d_3 \cong 8$, $d_5 \cong 116$, and b_n are the bunching coefficients, induced by the fundamental tone. They evolve along the z-coordinate as follows, $b_n^2(z) \cong h_n^2\left[P_1(z)/P_e\,\rho_1\right]^n$ (Huang & Kim, 2000), where the constants $h_{1,2,3,4,5} \cong \{1, 1.5, 2.4, 4.3, 7.7\}$ provide the agreement between their evolution and that of the proper power Q_n. The phenomenological coefficients d_i and h_i ensure better agreement with 3D models and FEL experiments. The full harmonic power includes both linear and non-linear terms: $P_n = P_{L,n} + Q_n$. The above-described evolution of the harmonic power is the result of the evolution of the bunching, which in the framework of the phenomenological model can be approximated by another logistic function (Dattoli & Ottaviani, 2002). The original formula from Dattoli & Ottaviani (2002) should be slightly modified to better describe the saturation region. For an unbunched beam the effective coupling power is $\sim$1/9 of the initial power (McNeil & Thompson, 2010; Pellegrini *et al.*, 2016; Schmüser *et al.*, 2014), and the bunching coefficients in an initially unbunched beam evolve to unity as follows,

$$B_n(z) = b_n^2(z) = \frac{n^{2/3}P_{n,0}}{P_e\,\rho_n}\,\frac{B(n,z)}{1 + B(n,z)\,P_{n,0}/P_{n,F}}, \tag{4}$$

$$B(n,z) = 2\left|\cosh\frac{z}{L_{n,g}} - \frac{\cos\left(z/L_{n,g} + z\sqrt{3}/2L_{n,g}\right)}{\exp\left(z/2L_{n,g}\right)} - \exp\left(\frac{z}{2L_{n,g}}\right)\cos\left(\frac{\pi}{3} - \frac{z\sqrt{3}}{2L_{n,g}}\right)\right|.$$

In a prebunched beam their evolution proceeds as follows,

$$B_n(z) = B_{n,0}\,\frac{G(n,z)}{1 + B_{n,0}[G(n,z) - 1]}, \tag{5}$$

$$G(n,z) = \cosh\frac{z}{L_{n,g}} + \sin\frac{z}{L_{n,g}}\cosh\frac{z}{2L_{n,g}},$$

where $B_{n,0}$ are the bunching coefficients for the electrons entering the FEL section. In either case a non-linear bunching term, induced by the dominant FEL harmonic, must be accounted for. The bunching coefficients evolution (5) yields the radiation power growth (2). Generalizing (Dattoli *et al.*, 2005), we write for the evolution of the bunching of the nth sub-harmonic, induced by the mth harmonic: $B_{n,\mathrm{induced}}(z) \cong h_n^2[P_m(z)/P_e\rho_m]^n$, which evidently reduces to the above-cited expression $b_n^2(z) \cong h_n^2[P_1(z)/P_e\,\rho_1]^n$ from Huang & Kim (2000).

3. Phenomenological description of the losses in real single-pass FELs

The above expressions describe the evolution of the bunching and power in an ideal multi-section single-pass FEL. However, to establish the agreement between the phenomenological theory and the experiment, losses should be accounted for. The coupling losses between the sections can be easily accounted for by the coefficients for the initial harmonic power and bunching; they depend on the technical construction and specific device and can be as high as 30%. Due to the eminent beam diffraction the Pierce parameter changes as follows (Dattoli *et al.*, 2005),

$$\rho_n \to \rho_{D,n} = \frac{\rho_n}{\left(1 + \mu_{D,n}\right)^{1/3}}, \qquad \mu_{D,n} = \frac{\lambda_u\lambda_n}{16\pi\rho_n\Sigma}, \tag{6}$$

where $\Sigma = P_e/(E_e\gamma J)$ is the cross section of the electron beam [m^2], $E_e = m_e c^2 \cong 0.511 \times 10^6$ is the electron rest energy [eV], P_e is the electron beam power [W], $J = I_0/\Sigma$ is the current density of the beam [A m^{-2}] and I_0 is the electron current [A]. Moreover, the electron–radiation interaction of

harmonics is more sensitive to the losses, beam divergences *etc.*, than the interaction at the fundamental frequency (Schneidmiller & Yurkov, 2012; Zhukovsky, 2015*c*, 2016*b*). Improvements with respect to the earlier (Zhukovsky & Potapov, 2017) description can be made by accounting for the interaction and losses individually at each harmonic wavelength (Zhukovsky, 2017*b*,*c*). Due to the beam energy spread and divergence the saturation length extends and the saturation power decreases as described by the following the phenomenological formulae,

$$L_{n,\mathrm{g}} \to L_{n,\mathrm{g}}\Phi_n, \qquad P_{n,F} \to P_{n,F}\,\eta_n, \tag{7}$$

$$\Phi_n \cong \left(\zeta^{n^{1/2}} + 0.165\mu_{\varepsilon,n}^2\right)\exp\left(0.034\mu_{\varepsilon,n}^2\right),$$
$$\eta_n \cong \frac{\exp\left[-\Phi_n(\Phi_n - 0.9)\right] + 1.57(\Phi_n - 0.9)/\Phi_n^3}{1.062}, \tag{8}$$

where $\mu_{\varepsilon,n}$ are the energy spread broadening coefficients for the nth harmonic,

$$\mu_{\varepsilon,n}(\sigma_\varepsilon, n) \cong 2n^{2/3}\,\sigma_\varepsilon/\rho_n. \tag{9}$$

The dependence of Φ_n and η_n (8) on the Twiss parameters $\beta_{x,y}$ and on the beam emittances $\varepsilon_{x,y}$ is cumbersome (Dattoli *et al.*, 2004; Xie, 2000). An approximate account for it,

$$\zeta \cong \left[\prod_{i=x,y,\tilde{x},\tilde{y}}\left(1+\mu_i^2\right)\right]^{1/2}\Bigg/\left(1 + 0.159\sum_{i=x,y,\tilde{x},\tilde{y}}\mu_i^2 - 0.066\sum_{i=x,y,\tilde{x},\tilde{y}}\mu_i\right),$$
$$\zeta|_{\mu_{\tilde{x},\tilde{y}}\ll 1} \simeq 1 + 0.07\sum_{i=x,y}\mu_i + 0.35\sum_{i=x,y}\mu_i^2, \tag{10}$$

improves our earlier description (Zhukovsky, 2017*b*,*c*) and brings it into agreement with the high-precision fitting formula of Xie (2000). For a matched beam we have $\zeta \simeq 1$–1.1. We use the formula from Dattoli *et al.* (2004), which relates the broadening coefficients μ_i to the relativistic parameter γ of the beam, its emittances $\varepsilon_{x,y}$, Twiss parameters $\beta_{x,y}$, the undulator parameter k and the number N of the undulator periods λ_u,

$$\mu_{x,y} = \frac{4N\gamma^2\varepsilon_{x,y}}{\beta_{x,y}(1+k^2/2)}, \qquad \mu_{\tilde{x},\tilde{y}} = \frac{4N\pi^2k^2\beta_{x,y}\varepsilon_{x,y}}{\lambda_\mathrm{u}^2(1+k^2/2)}. \tag{11}$$

Stable amplification in a FEL occurs if the beam energy spread and divergences are low, $\sigma_\varepsilon \le \rho/2$, $\varepsilon_{x,y} \le \lambda_0/4\pi$ (see, for example, Saldin *et al.*, 2000; Schmüser *et al.*, 2014). In an X-ray FEL, for reasonable values of the Twiss parameter and $\rho \simeq 10^{-3}$, we obtain $\zeta \simeq 1.0$–1.05. Moreover, even for longer-wave radiation, for example, with $\lambda \simeq 100$ nm in the PALADIN experiment (Winick *et al.*, 1994), where $\rho = 0.01$, $\beta_{x,y} > 2.5$ m, we have $\zeta \simeq 1.03$–1.05 (see Fig. 1).

Eminent axial asymmetry of the beam in a planar undulator can be also accounted for phenomenologically. This asymmetry is demonstrated by the example shown in Fig. 2, which we produced using the *SPECTRA* (Tanaka & Kitamura, 2001; Tanaka, 2014) numerical code. We omit the details for brevity.

Different from each other, x,y divergences and beam sizes are accounted for by $\varepsilon_{x,y}$. A separate account for the diffraction in each dimension can also be made with the help of the modified formula (6), published by Dattoli *et al.* (2004). The corrections for the axial asymmetry complement our phenomenological description. Further refinements of the corrections due to the losses can be made with the help of the high-precision fitting formulae of Xie (2000).

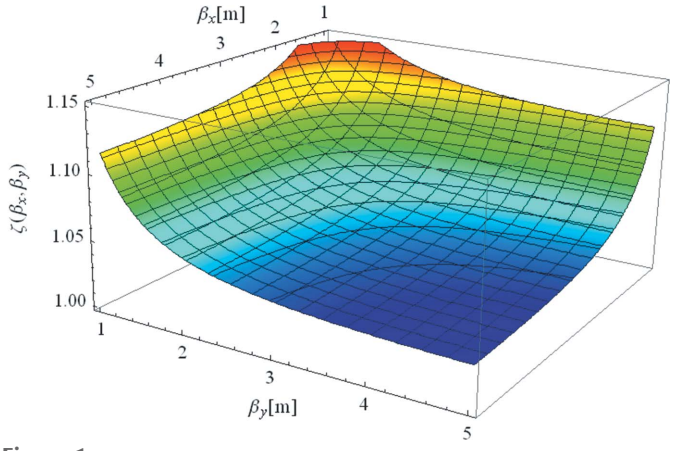

Figure 1
ζ-function in equation (10) for the Twiss parameters $\beta_{x,y}$ [m].

The above formulae (1)–(5) describe the case when the fundamental FEL harmonic is the strongest. However, in some special cases the harmonic n can dominate and the fundamental tone can be suppressed (Schneidmiller & Yurkov, 2012). In these cases the nth harmonic power evolution along the z coordinate is no longer limited by the saturation of the fundamental tone at Z_s and the power growth continues to the naturally saturated power $P_{F,n} \cong \sqrt{2}\rho_n P_\mathrm{e}$; with account for the losses we find

$$P_n^\mathrm{sat} = P_{F,n,D} \cong \sqrt{2}\left(\rho_{D,n}\right)^2 P_\mathrm{e}\eta_n/\rho_n.$$

The latter can be much higher than

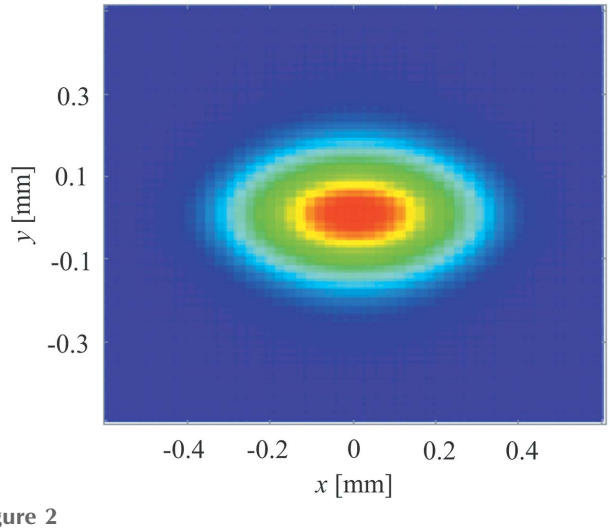

Figure 2
Axially asymmetric spatial distribution of the UR intensity modelled with the *SPECTRA* code in relative units; red, maximum intensity; blue, minimum.

$$P_{n,F} = \frac{P_F}{\sqrt{n}}\left(\frac{f_n}{nf_1}\right)^2.$$

Thus the nth harmonic can dominate and even induce nonlinear generation to its sub-harmonics. To adopt our phenomenological formalism to this case we use $L_{n,g}$ instead of L_g in (3); for the mth sub-harmonic, induced by the nth harmonic, we obtain the saturated power

$$P_{m\times n,F,D} = \frac{P_{F,n,D}}{\sqrt{m}}\left(\frac{f_{m\times n}}{mf_n}\right)^2 \eta_m$$

and bunching

$$b_{m\times n}(z) \cong h_m\left[P_n(z)/P_e\rho_{D,m\times n}\right]^{m/2}.$$

These expressions should be used for sub-harmonics instead of formulae (2)–(5) for harmonics. Note that the Pierce parameter and the Bessel coefficients f_m for sub-harmonics are very small in common planar undulators; therefore the sub-harmonic generation can be efficient only in two-frequency undulators.

The radiation interacting with the electrons increases the initial energy spread of the beam $\sigma_{\varepsilon,0}$ by the additional FEL-induced energy spread $\sigma_{\rm FEL}$. The energy spread induced by the fundamental harmonic was described phenomenologically by Dattoli & Ottaviani (2002). For the energy spread induced by the nth harmonic we modify that formula accordingly,

$$\sigma_\varepsilon^2(z) = \sigma_{\varepsilon,0}^2 + \frac{3}{2}\left\{\frac{\rho_{D,n}P_{0,n}A(n,z)\big|_{\rho\to\rho_{D,n}}/P_e}{1+1.24\left[A(n,z)\big|_{\rho\to\rho_{D,n}}-1\right]P_{0,n}/P_{F,n,D}}\right\}^{1/2}. \quad (12)$$

For the dominant fundamental harmonic, formula (12) applies with $n = 1$. Above we have given the phenomenological description of the evolution of the harmonic power and bunching in a single-pass FEL accounting for all major losses.

In the following we will demonstrate that in its present form the phenomenological model provides consistent agreement with an array of experimental results and it has a good match with numerical simulations, such as *PERSEO* (Gianessi, 2006). We will test the phenomenological model with PALADIN (Winick *et al.*, 1994) and other experiments (Freund *et al.*, 2000; Emma *et al.*, 2010), and compare with the results of *PERSEO* simulations and with experimental data. Then we will apply the phenomenological description to harmonic bunching and power modelling in the case of suppressed low-harmonics in a segmented two-frequency X-ray FEL undulator.

4. Comparative analysis of the harmonic power evolution in the PALADIN experiment with phenomenological and *PERSEO* simulations

In this section we will model the power evolution in some FEL experiments in the framework of the phenomenological approach and compare with numerical simulations using *PERSEO* codes (Gianessi, 2006) and with experimental reports. A comparison between the phenomenological model and an experiment at SPARC (Gianessi *et al.*, 2011) was made earlier by Zhukovsky & Potapov (2017). Good agreement of the experimental values for the fundamental and third harmonics was observed for the phenomenological model. It was actually better than that for some numerical simulations. Let us consider now the PALADIN experiment (Winick *et al.*, 1994), where the beam had an energy spread $\sigma_e = 2\times10^{-4}$, current $I_0 = 2000$ A, normalized emittances $\varepsilon_{x,y} = 3.5\times10^{-6}$ m rad and three different values of the relativistic parameter, $\gamma = \{1000, 2000, 3000\}$ (for more details, see Winick *et al.*, 1994). We estimated the beam cross sections, $\Sigma \simeq \{2.1\times10^{-7}, 1.05\times10^{-7}, 7.0\times10^{-8}\}$ m^2 and the initial coherent noise power values, $p_0 \simeq \{0.8, 8, 30\}$ kW, for the respective values $\gamma = \{1000, 2000, 3000\}$. The FEL had a rather strong undulator with $k = 4.1$ and long period $\lambda_u = 8$ cm. Comparison of the phenomenological modelling with the *PERSEO* numerical modelling for $\gamma = 1000$ is shown in Fig. 3, and for $\gamma = 2000$ in Fig. 4. Harmonics in the phenomenological model are denoted in thin solid lines: $n = 1$, red; $n = 3$, green; $n = 5$, blue. Harmonics in the *PERSEO* numerical model are denoted as follows: $n = 1$, thick solid black line; $n = 3$, dotted blue line; $n = 5$, dashed red line. The saturation length computed with the *PERSEO* code appears somewhat shorter than in the phenomenological model.

The experimental results for the saturation were reported at ∼11 m in the low-energy case (see modelling in Fig. 3) and at ∼18 m in the medium-energy case (see modelling in Fig. 4). The *PERSEO* code predicts ∼10.5 m and ∼15.5 m saturation lengths; the phenomenological model gives ∼11.5 m for the low-energy case (see Fig. 3) and 16.5 m for the medium-energy case (see Fig. 4), which is also close to the experimental 11 m and 18 m. In the high-energy case, $\gamma = 3000$, the match was good too; we omit proper figures for brevity. The saturated powers in both phenomenological and *PERSEO* numerical simulations were ∼10 GW, which exceeds the experimental value ∼5 GW. Peak harmonic powers agree fairly well in phenomenological and *PERSEO* simulations; oscillations are modelled only in *PERSEO*. Some discrepancy is natural even for complicated 3D simulations, performed, for example, for a SPARC experiment (Gianessi *et al.*, 2011), where a rather large disagreement between the results of different codes occurred. In our case, despite some disagreement in saturated power values and some shorter saturated length in *PERSEO*, both models reproduce quite well the power dynamics in PALADIN, with the phenomenological model giving a saturation length value closer to the experimental one.

Similarly a good match was observed with the results reported by Freund *et al.* (2000). We omit its discussion for conciseness. Moreover, we have applied our model to the study of the short-wave 1.5 Å FEL radiation in an LCLS experiment (Emma *et al.*, 2010). There, a very high energy electron beam with $\gamma = 26600$ and 3 kA current was used for generating sub-nanometric radiation at $\lambda = 0.15$ nm in the FEL undulator with a period $\lambda_u = 3$ cm and $k = 3.5$. The energy spread was reported as $\sigma_\varepsilon = 1\times10^{-4}$ and the normalized emittances were $\varepsilon_{x,y} = 0.4$ μm rad. The saturation was reported

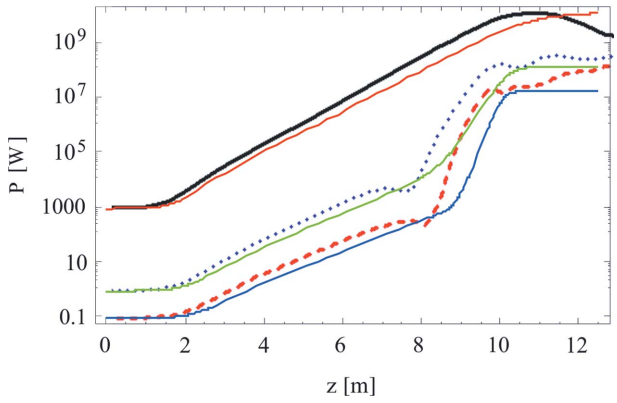

Figure 3
Comparison of the phenomenological and numerical *PERSEO* modelling of harmonic power in the PALADIN experiment for low energy, $\gamma = 1000$. Harmonics in the phenomenological model (thin solid lines): $n = 1$, red; $n = 3$, green; $n = 5$, blue. Harmonics in the *PERSEO* model: $n = 1$, thick solid black line; $n = 3$, dotted blue line; $n = 5$, dashed red line.

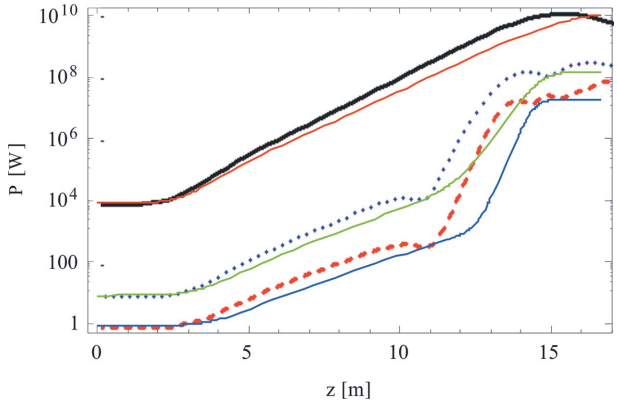

Figure 4
Comparison of the phenomenological and numerical *PERSEO* modelling of the harmonic power in the PALADIN experiment for medium energy, $\gamma = 2000$. Harmonics in the phenomenological model (thin solid lines): $n = 1$, red; $n = 3$, green; $n = 5$, blue. Harmonics in the *PERSEO* model: $n = 1$, thick solid black line; $n = 3$, dotted blue line; $n = 5$, dashed red line.

at 60 m with ∼12 GW power; the gain length at the facility was calculated to be ∼4 m and experimentally measured at 3.5 m (Emma *et al.*, 2010). We reproduced the power growth in that FEL by means of a numerical simulation using the *PERSEO* code and in the framework of our phenomenological model. The FEL power evolution is graphically presented in Fig. 5.

Our phenomenological model predicts the saturation at 56 m of pure undulator length, which is in very good agreement with the reported value if we account for 15 cm gaps between 17 undulator segments, each 3.4 m long. We have obtained a gain length $L_{\rm gain} = 3.8$ m in the phenomenological model, which also fits very well the interval 3.5–4 m reported by Emma *et al.* (2010) and is even closer to the measured 3.5 m value than the 4 m theoretical estimation of the installation design. The saturated power peaks at 22 GW in the phenomenological model, which also agrees with our numerical simulation using *PERSEO* and with the average measured

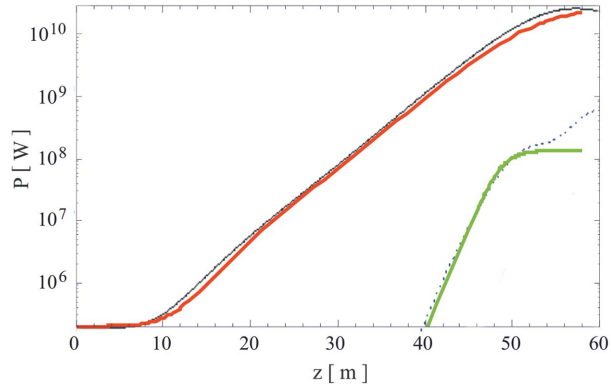

Figure 5
Comparison of the phenomenological and numerical *PERSEO* modelling of the harmonic power in the 1.5 Å FEL radiation experiment for $\gamma = 26600$, $\sigma_\varepsilon = 1 \times 10^{-4}$, $\varepsilon_{x,y} = 0.4$ µm, $\lambda_{\rm u} = 3$ cm, $k = 3.5$. Harmonics in the phenomenological model (thick solid lines): $n = 1$, red; $n = 3$, green. Harmonics in the *PERSEO* model (thin lines): $n = 1$, solid black line; $n = 3$, dotted blue line.

value of 12 GW taking into account oscillations of the saturated power. The latter phenomenon remains beyond our phenomenological model, which describes just the initial saturation. The average saturated power of the fundamental harmonic appears somewhat lower due to its oscillations, while the high-harmonics power also oscillates and keeps growing for a while at a lower rate in the saturated regime (see the *PERSEO* numerical simulation in Figs. 3–5).

Note that the requirement $\varepsilon_{x,y} \leq \lambda_0/4\pi$ is hardly fulfilled in X-ray FELs. Even for the fundamental harmonic in the LCLS experiment (Emma *et al.*, 2010) the condition is barely satisfied, $\varepsilon \cong \lambda_0/4\pi \cong 1.2 \times 10^{-11}$, and for the third harmonic the inequality just does not hold. For this reason high harmonics were not registered in the LCLS experiment. The absence of high harmonics in FELs, where the fundamental tone is in the X-ray band, is rather common; we have shown the third harmonic in Fig. 5 to demonstrate that the phenomenological model agrees with the numerical one. In the PALADIN experiment the conditions for the radiation of the third and fifth harmonics were satisfied.

The above comparison of the phenomenological approach, numerical *PERSEO* code and measurements shows consistently good agreement in various experiments at different facilities under different conditions and at different radiation wavelengths, ranging from hundreds of nanometres to 1.5 Å. This is a good result, in particular taking into account that only a few basic parameters are needed for the phenomenological model.

5. Two-frequency planar undulator in a single-pass FEL

It was demonstrated (Zhukovsky, 2014, 2015*a*,*b*, 2016*a*) that much stronger UR harmonics can be obtained in a planar undulator with the following double-period magnetic field,

$$\mathbf{H} = \left\{0, H_0\left[\sin(k_\lambda z) + d\sin(hk_\lambda z)\right], 0\right\}, \qquad (13)$$

where $k_\lambda = 2\pi/\lambda_u$, $h \in Z$, $d, h =$ constant, than in a common planar undulator. The radiation from the undulator with the field (13) has the wavelength

$$\lambda_n = \frac{\lambda_u}{2n\gamma^2}\left(1 + \frac{k_{eff}^2}{2}\right),$$

where $k_{eff}^2 = k^2 + k_2^2$ and $k_2 = k|d/h|$. For a common planar undulator it is enough to set $d = 0$. The Bessel coefficients $f_{n,x}$ for the FEL undulator with the field (13) depend on the generalized Bessel functions $I_n^{(h)}$ (Zhukovsky, 2016*b*). They have the following integral presentation (Dattoli *et al.*, 2006),

$$\begin{aligned} f_{n,x} &= I_{n-1}^{(h)} + I_{n+1}^{(h)} + (d/h)\left[I_{n+h}^{(h)} + I_{n-h}^{(h)}\right], \\ I_n^{(h)} &= \int_0^{2\pi} \cos\left[n\varphi + \frac{k^2(\xi_1 + \xi_2 + \xi_3 + \xi_4)}{1 + k_{eff}^2/2}\right]\frac{d\varphi}{2\pi}, \\ \xi_1 &= \frac{\sin(2\varphi)}{4}, \qquad \xi_2 = -\frac{d\sin[(h-1)\varphi]}{h(h-1)}, \\ \xi_3 &= -\frac{d\sin[(h+1)\varphi]}{h(h+1)}, \qquad \xi_4 = -\frac{d^2\sin(2h\varphi)}{4h^3}. \end{aligned} \tag{14}$$

Some simulations for a FEL with a two-frequency undulator were carried out by Dattoli *et al.* (2006); and two-colour radiation was modeled with a crossed two-frequency undulator (Dattoli *et al.*, 2014). Recently harmonic generation and evolution in two-frequency FEL undulators was studied by Zhukovsky & Potapov (2017); modelling showed that the bunching coefficients for high harmonics in a two-frequency FEL with low electron energy spread ($\sigma_\varepsilon = 0.0001$) evolved in a linear regime, following the bunching at the fundamental wavelength; lasing of high harmonics occurred mostly due to independent bunching at their wavelengths λ_n. For a common planar undulator, on the contrary, everything depends on the fundamental harmonic, which largely induces bunching for high harmonics. The latter appear much weaker than in a two-frequency undulator. The harmonic bunching coefficients in a common planar undulator grow slower than in a two-frequency undulator until nonlinear growth kicks in, induced by the fundamental harmonic (for details, see Zhukovsky & Potapov, 2017). This inspired a proposal to use two-frequency undulators–prebunchers in cascaded HGHG FELs (Zhukovsky, 2017*a*,*b*,*c*, 2018*a*,*b*,*c*) to group electrons directly at the harmonic wavelengths with high bunching values in linear growth. It was shown that high power of FEL harmonics could be achieved in such FELs over a short length.

6. High-harmonic saturated power increase and low-harmonic suppression

A two-frequency undulator with proper secondary periodic field can provide much stronger high harmonics than a common planar undulator. However, its exponential harmonic power growth is nevertheless limited by the saturation of the first harmonic. The latter induces significant electron energy spread and prevents high harmonics from growing further along the FEL. Thus, high harmonics saturate approximately at the same length with the fundamental or some earlier harmonic (Deng & Dai, 2013; Bonifacio *et al.*, 1990; Huang & Kim, 2000; Schneidmiller & Yurkov, 2012). Their power and bunching evolution is fairly well described in §2. In order to boost high harmonics to the maximum power, they should grow beyond the saturation length of the fundamental harmonic. Various methods were proposed, such as filtering off the radiation of the fundamental tone and phase-shifting the electrons to the radiation between the undulator cascades (Schneidmiller & Yurkov, 2012; McNeil *et al.*, 2006). The shift by $k\pi/n$, where k = 2, 4, 6, *etc.*, of $2\pi/n$ or $4\pi/n$ interrupts otherwise continuous growth of the bunching in the FEL by displacing the position of the electron micro-bunch from the nodes of the radiation field of the fundamental harmonic. This $k\pi/n$ phase shift, however, does not alter the harmonic field interaction with the electron micro-bunches and thus exponential growth of the nth harmonic power proceeds along the FEL even beyond the saturation length of the fundamental tone. Moreover, a weak fundamental tone induces a smaller energy spread. This phenomena has been explored in common undulators by Schneidmiller & Yurkov (2012) and McNeil *et al.* (2006).

In this study we explore the harmonic growth in a phase-shifted FEL with the two-frequency undulator. For this purpose we use a simple phenomenological description, where the possibility of a high harmonic, dominating over the fundamental one, is included (see §3). Consider, for example, the electrons mismatched to the photons of the fundamental tone by $2\pi/5$ between the undulator cascades. This phase shift neither alters the bunching at the fifth FEL harmonic wavelength nor attenuates the radiation between the undulator sections. However, this repetitive phase shift makes the electrons rebunch at the fundamental wavelength after each section. In our example we assumed the electron energy E = 5.47 GeV, γ = 10700, low beam energy spread $\sigma_\varepsilon = 0.0001$ and high current $I_0 \simeq 3.66$ kA, which is typical for modern FEL orders of magnitude (McNeil & Thompson, 2010; Pellegrini *et al.*, 2016; Pellegrini, 2016). We assume ~15% coupling losses between the undulator cascades. Further data are collected in Table 1.

The disruption of the bunching evolution for the fundamental harmonic of the phase-shifted two-frequency FEL is shown in Fig. 6 (see red lines). The growth of the bunching coefficient for the fundamental harmonic is interrupted after each section due to the imposed phase shift, which displaces the electrons away from the wave nodes of the fundamental tone. The electrons start regrouping in this beam, which is effectively debunched at the harmonic wavelength. In this process only ~1/9 of the radiation power between the cascades couples to the unbunched electrons (Pellegrini *et al.*, 2016; Huang & Kim, 2007; Saldin *et al.*, 2000). For bunched electrons the coupling losses usually do not exceed 20–25%. The repetitive process of disruption of the bunching and consequent rebunching in the phase-shifted FEL does not allow the fundamental harmonic to reach its usual high output power. Similar considerations regarding the third harmonic are denoted by the green piecewise line in Fig. 6.

Table 1
Modelling data for the FEL with the two-frequency undulator and suppressed low-harmonics; the dominating fifth harmonic wavelength equals 0.15 nm (see Figs. 6 and 7) and matches the fundamental radiation wavelength in the LCLS experiment (Emma *et al.*, 2010).

Electron beam characteristics	$\gamma = 10700$, $\sigma_e = 0.0001$, $J = 3.125 \times 10^{11}$ A m^{-2}, $\Sigma = 1.17 \times 10^{-8}$ m^2, $I_0 = 3.66$ kA, $P_E = 20000$ GW, $\zeta = 1.04$
FEL undulator properties and relevant parameters	$\lambda_u = 2.8$ cm, $k = 3.2$, $h = 3$, $d = -0.5$, $L_s = 26$ m, $L_{s5} = 30$ m, $L_{gain} = 1.8$ m
Radiation related parameters	$\lambda_{n=1} = 0.76$ nm, $\lambda_{n=3} = 0.25$ nm, $\lambda_{n=5} = 0.15$ nm, $\lambda_{n=5\times3} = 0.05$ nm, $\lambda_{n=5\times5} = 0.03$ nm, $P_{F5} = 14$ GW, $P_{n=1,3} = 13$ MW, $P_{n=5,F} = 0.25$ GW, $P_{n=5\times3}^{sat} = 0.25$ GW, $P_{n=5\times5}^{sat} = 13$ MW

Harmonic number	$n = 1$	$n = 3$	$n = 5$
f_n	0.6118	0.4763	0.4182
$\rho_{D,n}$	0.000753	0.000643	0.000591

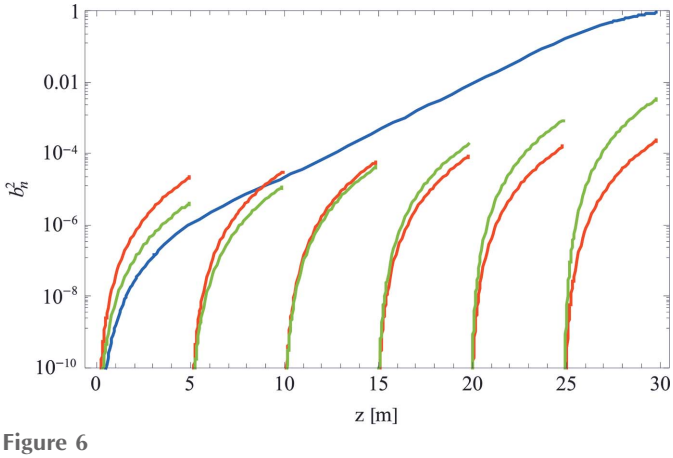

Figure 6
Evolution of the harmonic bunching coefficients in a FEL with the two-frequency undulator, where rebunching at the fundamental harmonic wavelength is induced after each undulator section. Bunching coefficients for the harmonic with $n = 1$, red lines; for the harmonic with $n = 3$, green lines; $n = 5$, blue line.

The more frequently the phase-shifters are placed, the better the suppression of low harmonics becomes. Undisturbed growth of the fifth-harmonic bunching is denoted by the blue line in Fig. 6. It demonstrates that the bunching at the fifth-harmonic wavelength grows continuously along the whole FEL. The respective FEL harmonic power evolution is shown in Fig. 7, where we observe the disruption of the exponential growth of the low-harmonics radiation power; the fundamental-harmonic power is denoted by the red line, and the third-harmonic power is denoted by the green line.

In Fig. 7, short-dashed red, green and blue lines denote the powers of the harmonics with $n = 1, 3$ and 5, respectively, in the two-frequency FEL without the phase shift. Solid lines in Fig. 6 describe the harmonic power evolution, following the bunching evolution, simulated in Fig. 6. The disruption of the bunching for the harmonics with $n = 1$ and $n = 3$ (see Fig. 6) affects the respective harmonic powers, denoted by the red and green lines in Fig. 7: their piecewise growth leads to lower

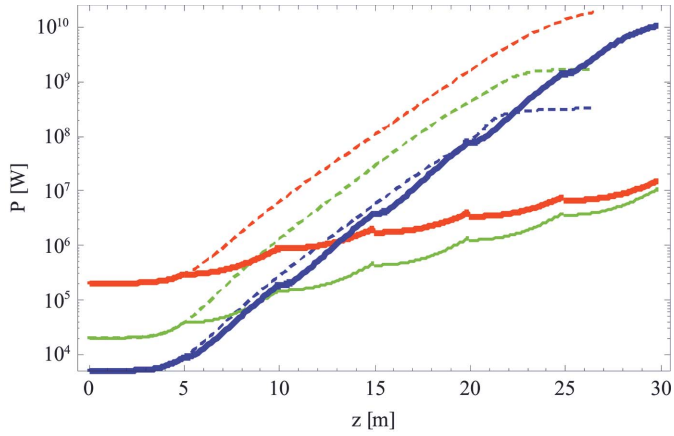

Figure 7
FEL harmonic power evolution. The harmonic power in the phase-shifted two-frequency FEL undulator is shown by the solid lines; the common case, when the fundamental harmonic dominates, is shown by short-dashed lines. The harmonics with $n = 1$, 3 and 5 are denoted by the red, green and blue lines, respectively.

output power. The fifth harmonic, denoted by the solid blue line in Fig. 7, grows after the 20 m point, where the saturation otherwise occurred (short-dashed blue line), and it becomes dominant towards the end of the phase-shifted FEL with the saturation power $P_{F5} \cong \sqrt{2}(\rho_{D,5}^2/\rho_5)\, P_e\, \eta_5$. The latter is higher than the output power of the fundamental tone in this phase-shifted FEL (see Fig. 7). Indeed, as shown in Fig. 7, the fifth harmonic at $\lambda_{n=5} = 0.15$ nm saturates after 30 m *versus* 20 m in the non-shifted FEL, and reaches $\sim$14 GW *versus* $\sim$0.3 GW saturated power in the non-shifted FEL. Moreover, the fifth harmonic in the phase-shifted FEL has the same wavelength, 0.15 nm, as the fundamental harmonic of the LCLS FEL (Emma *et al.*, 2010) (see §4), and has a similar saturated power to the LCLS FEL, $\sim$20 GW. It is achieved at a much shorter FEL length, $\sim$30 m, which is a half of the LCLS ($\sim$60 m) FEL saturation length (compare the blue solid line in Fig. 7 with the red line in Fig. 5). The fifth harmonic in the common planar undulator [$d = 0$ in (13)] is significantly weaker than in the two-frequency undulator and we omit it's plot in Fig. 7 for clarity. In our simulation we have assumed complete debunching of the electrons at the first- and third-harmonic wavelengths between the undulator sections due to the phase shift. If the debunching is partial, the suppression of proper harmonics is weaker. In this case we obtained results similar to those reported in Fig. 7, but we obtained higher powers of the first and third harmonics, reaching $\sim 10^8$ W (we omit the figures for brevity), *i.e.* ten times higher than those shown in Fig. 7. Nevertheless, in this case the first and third harmonic powers remain $\sim$100 times lower than the power of the dominant fifth harmonic, which reaches 10^{10} W.

In the FEL with the two-frequency undulator and suppressed low harmonics, the fifth harmonic dominates (solid blue line in Figs. 7 and 8) and can induce higher sub-harmonics in the non-linear regime, similarly to that of a strong fundamental harmonic in a common undulator FEL. In Fig. 8 we show that the dominant harmonic with $n = 5$ induces after 22 m the third sub-harmonic at 0.05 nm (see the dashed line in

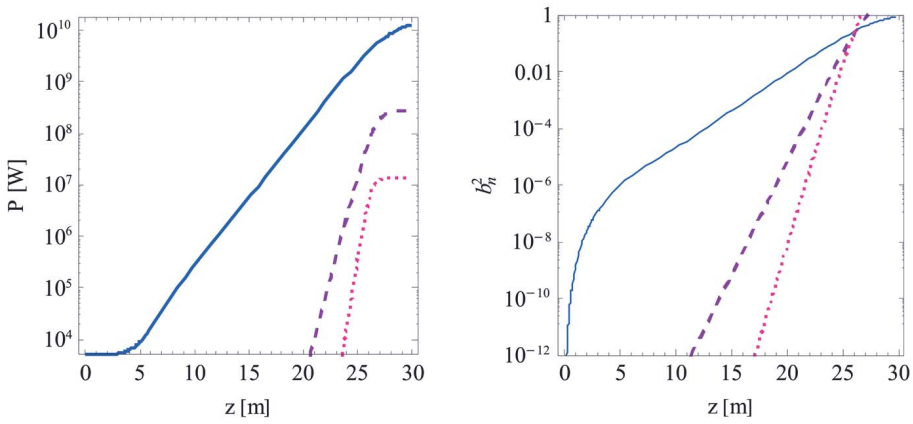

Figure 8
Evolution of the subharmonic power (left) and bunching (right), induced by the dominant fifth harmonic. Dashed and dotted lines denote the third and fifth sub-harmonics, respectively, induced by the fifth harmonic (blue solid line).

Fig. 8); it has a relatively high saturated power, ∼0.25 GW, comparable with the power of the fundamental tone (see Fig. 7).

Even the fifth sub-harmonic at 0.03 nm can appear after 27 m if the emittance of the electron beam is sufficiently low; then it can reach ∼13 MW power (see the dotted line in Fig. 8). Such sub-harmonic generation can occur in the two-frequency FEL with suppressed low-harmonics and is very weak in the common undulator FEL because the latter has very small values for the Pierce parameter and Bessel coefficients for high harmonics. Moreover, for the sub-harmonic generation to occur, the fundamental FEL tone should be suppressed for the high-harmonics benefit and the energy spread and the emittance must be very low. For example, for the sub-harmonic at 0.05 nm we have $\lambda_0/4\pi \cong 4 \times 10^{-12}$ m rad, which gives a normalized emittance estimation $\varepsilon \cong 0.04$ mm mrad, which is a very small value. Thus, sub-harmonics can be detected only in very high quality installations.

If the fundamental harmonic is suppressed, the dominant high-harmonic induces the energy spread. We compared the induced electron energy spread in a two-frequency FEL with the dominant fifth harmonic (solid line in the left-hand plot in Fig. 9) and dominant fundamental harmonic (dashed line in the left-hand plot in Fig. 9). The ratio of the proper values $\sigma_{\varepsilon,n=1}/\sigma_{\varepsilon,n=5}$ is shown in the right-hand plot in Fig. 9.

The FEL with the dominant fifth harmonic induces less energy spread after 15 m than the FEL with the dominant fundamental harmonic (compare the solid and dashed lines in the left-hand plot in Fig. 9). The difference in the induced energy spread becomes largest at ∼23 m, where the FEL with the dominant fifth harmonic has a three times lower total energy spread than the FEL with the dominant fundamental tone (see the right-hand plot in Fig. 9).

Thus, the suppression of low harmonics in a FEL, for example by the repetitive electrons–photons phase shift, makes it possible to obtain a powerful *n*th harmonic in a two-frequency undulator with significant, with respect to the common planar undulator, independent harmonic gain in the linear regime. The power of the *n*th harmonic in such a FEL can greatly exceed the power of its fundamental tone. Moreover, it can exceed the power of the fundamental tone in a common planar undulator, tuned at the same high-harmonic frequency, and it can also generate sub-harmonics in the nonlinear regime. The FEL-induced electron energy spread in such a FEL is several times less than in the FEL, where the fundamental tone usually dominates.

7. Results and conclusions

We have studied the FEL harmonic power and bunching evolution in the framework of the enhanced phenomenological model. We have performed simulations for PALADIN and other FEL experiments, with 0.5 µm to 0.15 nm radiation (Winick *et al.*, 1994; Freund *et al.*, 2000; Emma *et al.*, 2010) with the phenomenological model and with the *PERSEO* numerical code. A comparative analysis of the harmonic power in these experiments demonstrated that the phenomenological model, although it is based on few basic input parameters, reproduces the experimental data very well; up to the saturation point the agreement is even better than that with the numerical *PERSEO* code. We obtained a perfect match with the 1.5 Å FEL experiment (Emma *et al.*, 2010).

In order to show the advantage of two-frequency undulators in harmonic generation and independent harmonic

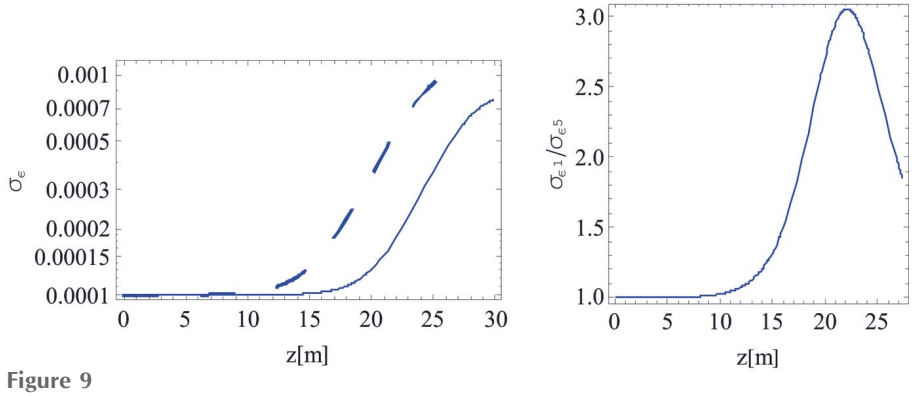

Figure 9
Evolution of the electron energy spread along the FEL; the dashed line describes the energy spread in the common FEL, solid lines describe the energy spread in the FEL, where low harmonics are suppressed and the fifth harmonic dominates. The right-hand plot shows the ratio of the energy spread in the common FEL with the dominant fundamental harmonic to that in the FEL with the dominant fifth harmonic.

growth in the linear regime we performed simulations for a cascaded FEL with the two-frequency undulator, where the low-harmonic growth was suppressed and the fifth harmonic was enhanced. Moreover, we have demonstrated that with the two-frequency undulator, having basic parameters of the undulator from Emma *et al.* (2010) and the additional second periodic magnetic field, it is possible to obtain similar radiation power and frequency as Emma *et al.* (2010) but on half of the FEL length, *i.e.* 30 m instead of 60 m, with less than half the electron energy, $\gamma = 10700$ instead of $\gamma = 2660$, for a similar beam current and other beam parameters. With electron energy $E = 5.47$ GeV and current $I_0 = 3.66$ kA we showed that 14 GW radiation can be obtained for the fifth harmonic at sub-nanometric wavelength $\lambda_5 = 0.15$ nm (see Fig. 7). The radiation power and wavelength are close to the proper values in the LCLS experiment (Emma *et al.*, 2010) under similar conditions, but the saturation length is twice as short as that for the FEL, radiating the fundamental harmonic in the common planar undulator (Emma *et al.*, 2010); moreover, the electron energy is now $E = 5.47$ GeV *versus* the $E = 13.6$ GeV of Emma *et al.* (2010). This shows that use of the two-frequency undulator requires a much lower electron energy and shorter FEL length.

Using a $k\pi/n$ phase shift for the electrons with respect to the photons between the undulator sections (Schneidmiller & Yurkov, 2012; McNeil *et al.*, 2006), it is possible to disrupt the bunching for harmonics lower than the nth. This allows the nth harmonic to grow even beyond the point where its saturation usually occurs, determined by the saturation of the fundamental tone. We have modelled this situation for the fifth harmonic in the two-frequency undulator with the help of the accordingly modified phenomenological model. We have demonstrated the disruption of the bunching for low harmonics (see Fig. 6) and a proper decrease of their harmonic power (see Fig. 7). In this case the fifth harmonic can dominate. Its evolution proceeds in a linear regime independent of the fundamental tone and its power can be boosted many dozens of times. To this end the electron beam should be of high quality.

In a compact FEL of $\sim$30 m with a two-frequency undulator and suppressed low harmonics, the dominant fifth harmonic can induce its third sub-harmonic at $\lambda_{n=5\times3} = 0.05$ nm with 270 MW power (dashed line in Fig. 7) and even the fifth sub-harmonic at $\lambda_{n=5\times5} = 0.03$ nm with 13 MW power (see Fig. 7). This is hardly possible in a common planar undulator because of the insufficient amplification of high harmonics and low values of the respective Bessel coefficients.

We have also shown that in a FEL with a two-frequency undulator and suppressed low harmonics the energy spread becomes three times smaller than in a common FEL, where the fundamental tone dominates. The difference is largest at the end of the FEL at the point where saturation usually occurs (see Fig. 9).

Thus, the suppression of low harmonics by the electrons-to-photons phase-shift boosts the maximum power of the fifth harmonic in the two-frequency X-ray FEL undulator to $\sim$13 GW at $\lambda_5 \simeq 0.15$ nm for an electron current of $\sim$3.66 kA; just 30 m are needed for this. Otherwise a twice-as-long common undulator FEL and 2.5 times higher electron energy are needed to obtain such radiation. Moreover, the generation of sub-harmonics with wavelengths <0.05 nm may be possible if the divergences are kept low. The considered compact FEL with the two-frequency undulator can complement existing large installations at a lower cost and smaller size.

Acknowledgements

The authors are grateful to Professor A. Borisov, Professor A. Vasiliev, Dr A. Lobanov and Professor V. Zhukovsky for useful discussions.

References

Albertin, F., Astolfo, A., Stampanoni, M., Peccenini, E., Hwu, Y., Kaplan, F. & Margaritondo, G. (2015). *X-ray Spectrom.* **44**, 93–98.
Bagrov, V. G., Bisnovaty-Kogan, G. S., Bordovitsyn, V. A., Borisov, A. V., Dorofeev, O. F., Epp, V. Ya., Pivovarov, Yu. L., Shorokhov, O. V. & Zhukovsky, V. Ch. (2002). *Radiation Theory of Relativistic Particles*, edited by V. A. Bordovitsyn. Moscow: Fizmatlit. (In Russian.)
Bajt, S. C. & Wall, M. A. (2000). PCT number PCT/US2000/013549.
Bajt, S. C. & Wall, M. A. (2002). Patent number EP 1198725A1.
Bonifacio, R., De Salvo, L. & Pierini, P. (1990). *Nucl. Instrum. Methods Phys. Res. A*, **293**, 627–629.
Bonifacio, R., Pellegrini, C. & Narducci, L. (1984). *Opt. Commun.* **50**, 373–378.
Colson, W. B. (1997). *Nucl. Instrum. Methods Phys. Res. A*, **393**, 82–85.
Dattoli, G. J. (1998). *J. Appl. Phys.* **84**, 2393–2398.
Dattoli, G., Giannessi, L., Ottaviani, P. L. & Ronsivalle, C. J. (2004). *J. Appl. Phys.* **95**, 3206–3210.
Dattoli, G., Mikhailin, V. V., Ottaviani, P. L. & Zhukovsky, K. J. (2006). *J. Appl. Phys.* **100**, 084507.
Dattoli, G., Mirian, N. S., DiPalma, E. & Petrillo, V. (2014). *Phys. Rev. ST Accel. Beams*, **17**, 050702.
Dattoli, G. & Ottaviani, P. L. (2002). *Opt. Commun.* **204**, 283–297.
Dattoli, G., Ottaviani, P. L. & Pagnutti, S. J. (2005). *J. Appl. Phys.* **97**, 113102.
De Martini, F. (1990). *Laser Handbook*, Vol. 6, edited by W. B. Colson, C. Pellegrini & A. Renieri, p. 195. Amsterdam: North-Holland.
Deng, H.-X. & Dai, Z.-M. (2010). *Chin. Phys. C*, **34**, 1140.
Deng, H.-X. & Dai, Z.-M. (2013). *Chin. Phys. C*, **37**, 102001.
Emma, P. *et al.* (2010). *Nat. Photon.*, **4**, 641–647.
Frank, M., Carlson, D. B., Hunter, M. S., Williams, G. J., Messerschmidt, M., Zatsepin, N. A., Barty, A., Benner, W. H., Chu, K., Graf, A. T., Hau-Riege, S. P., Kirian, R. A., Padeste, C., Pardini, T., Pedrini, B., Segelke, B., Seibert, M. M., Spence, J. C. H., Tsai, C.-J., Lane, S. M., Li, X.-D., Schertler, G., Boutet, S., Coleman, M. & Evans, J. E. (2014). *IUCrJ*, **1**, 95–100.
Freund, H. P., Biedron, S. G. & Milton, S. V. (2000). *Nucl. Instrum. Methods Phys. Res. A*, **445**, 53–58.
Gianessi, L. (2006). *Proceedings of 28th International Free Electron Laser Conference (FEL 2006)*, 27 August–1 September 2006, Berlin, Germany. MOPPH026
Giannessi, L. *et al.* (2011). *Phys. Rev. ST Accel. Beams*, **14**, 060712.
Ginzburg, V. L. (1947). *Izv. Akad. Nauk SSSR (Fiz.)*, **11**, 1651.
Huang, Z. & Kim, K.-J. (2000). *Phys. Rev. E*, **62**, 7295–7308.
Huang, Z. & Kim, K.-J. (2007). *Phys. Rev. ST Accel. Beams*, **10**, 034801.
Kim, K. J. & Xie, M. (1993). *Nucl. Instrum. Methods Phys. Res. A*, **331**, 359–364.

Kroll, N. M. & McMullin, W. A. (1978). *Phys. Rev. A*, **17**, 300–308.
Li, H.-T. & Jia, Q. K. (2013). *Chin. Phys. C*, **37**, 028102.
Margaritondo, G. (2015). *Synchrotron Radiation: Basics, Methods and Applications*, edited by S. Mobilio, F. Boscherini & C. Meneghini, pp. 29–63. Springer.
Margaritondo, G. (2017). *Riv. Nuov. Cim.* **40**, 411–471.
Margaritondo, G. & Rebernik Ribic, P. (2011). *J. Synchrotron Rad.* **18**, 101–108.
McNeil, B. (2008). *Nat. Photon.* **2**, 522–524.
McNeil, B. W. J., Robb, G. R. M., Poole, M. W. & Thompson, N. R. (2006). *Phys. Rev. Lett.* **96**, 084801.
McNeil, B. W. J. & Thompson, N. R. (2010). *Nat. Photon.* **4**, 814–821.
Mishra, G., Gehlot, M. & Hussain, J.-K. (2009). *Nucl. Instrum. Methods Phys. Res. A*, **603**, 495–503.
Motz, H., Thon, W. & Whitehurst, R. N. J. (1953). *J. Appl. Phys.* **24**, 826–833.
Onuki, H. & Elleaume, P. (2003). *Undulators, Wigglers and their Applications.* New York: Taylor & Francis.
Pellegrini, C. (2016). *Phys. Scr.* T**169**, 014004.
Pellegrini, C., Marinelli, A. & Reiche, S. (2016). *Rev. Mod. Phys.* **88**, 015006.
Quattromini, M., Artioli, M., Di Palma, E., Petralia, A. & Giannessi, L. (2012). *Phys. Rev. ST Accel. Beams*, **15**, 080704.
Saldin, E. L., Schneidmiller, E. A. & Yurkov, M. V. (2000). *The Physics of Free Electron Lasers.* Berlin: Springer.
Saldin, E. L., Schneidmiller, E. A. & Yurkov, M. V. (2002). *Opt. Commun.* **202**, 169–187.
Saldin, E. L., Schneidmiller, E. A. & Yurkov, M. V. (2010). *New J. Phys.* **12**, 035010.
Schmüser, P., Dohlus, M., Rossbach, J. & Behrens, C. (2014). *Free-Electron Lasers in the Ultraviolet and X-ray Regime*, Vol. 258 of *Springer Tracts in Modern Physics.* Heidelberg: Springer-Verlag.
Schneidmiller, E. A. & Yurkov, M. V. (2012). *Phys. Rev. ST Accel. Beams*, **15**, 080702.
Seddon, E. A., Clarke, J. A., Dunning, D. J., Masciovecchio, C., Milne, C. J., Parmigiani, F., Rugg, D., Spence, J. C. H., Thompson, N. R., Ueda, K., Vinko, S. M., Wark, J. S. & Wurth, W. (2017). *Rep. Prog. Phys.* **80**, 115901.
Shaftan, T. & Yu, L.-H. (2005). *Phys. Rev. E*, **71**, 046501.
Shintake, T. *et al.* (2008). *Nat. Photon.* **2**, 555–559.
Sprangle, P. & Smith, R. A. (1980). *Phys. Rev. A*, **21**, 293–301.
Tanaka, T. (2014). *Phys. Rev. ST Accel. Beams*, **17**, 060702.
Tanaka, T. & Kitamura, H. (2001). *J. Synchrotron Rad.* **8**, 1221–1228.
Tiedtke, K., Azima, A., von Bargen, N., Bittner, L., Bonfigt, S., Düsterer, S., Faatz, B., Frühling, U., Gensch, M., Gerth, C., Guerassimova, N., Hahn, U., Hans, T., Hesse, M., Honkavaar, K., Jastrow, U., Juranic, P., Kapitzki, S., Keitel, B., Kracht, T., Kuhlmann, M., Li, W. B., Martins, M., Núñez, T., Plönjes, E., Redlin, H., Saldin, E. L., Schneidmiller, E. A., Schneider, J. R., Schreiber, S., Stojanovic, N., Tavella, F., Toleikis, S., Treusch, R., Weigelt, H., Wellhöfer, M., Wabnitz, H., Yurkov, M. V. & Feldhaus, J. (2009). *New J. Phys.* **11**, 023029.
Vinokurov, N. A. & Levichev, E. B. (2015). *Phys. Usp.* **185**, 917–939.
Walker, R. P. (1993). *Nucl. Instrum. Methods Phys. Res. A*, **335**, 328–337.
Winick, H., Bane, K., Boyce, R., Cobb, J., Loew, G., Morton, P., Nuhn, H.-D., Paterson, J., Pianetta, P., Raubenheimer, T., Seeman, J., Tatchyn, R., Vylet, V., Pellegrini, C., Rosenzweig, J., Travish, G., Prosnitz, D., Scharlemann, E. T., Halbach, K., Kim, K.-J., Schlueter, R., Xie, M., Bonifacio, R., De Salvo, L. & Pierini, P. (1994). *Nucl. Instrum. Methods Phys. Res. A*, **347**, 199–205.
Xie, M. (2000). *Nucl. Instrum. Methods Phys. Res. A*, **445**, 59–66.
Yu, L.-H. (1991). *Phys. Rev. A*, **44**, 5178–5193.
Yu, L.-H., Babzien, M., Ben-Zvi, I., DiMauro, L. F., Doyuran, A., Graves, W., Johnson, E., Krinsky, S., Malone, R., Pogorelsky, I., Skaritka, J., Rakowsky, G., Solomon, L., Wang, X. J., Woodle, M., Yakimenko, V., Biedron, S. G., Galayda, J. N., Gluskin, E., Jagger, J., Sajaev, V. & Vasserman, I. (2000). *Science*, **289**, 932–935.
Yu, L.-H., DiMauro, L., Doyuran, A., Graves, W. S., Johnson, E. D., Heese, R., Krinsky, S., Loos, H., Murphy, J. B., Rakowsky, G., Rose, J., Shaftan, T., Sheehy, B., Skaritka, J., Wang, X. J. & Wu, Z. (2003). *Phys. Rev. Lett.* **91**, 074801.
Zeng, L., Qin, W., Zhao, G., Huang, S., Ding, Y., Huang, Z., Marcus, G. & Liu, K. (2016). *Chin. Phys. C*, **40**, 098102.
Zhukovsky, K. (2014). *J. Electromagn. Waves Appl.* **28**, 1869–1887.
Zhukovsky, K. (2015*a*). *Moscow Univ. Phys.* **70**, 232–239.
Zhukovsky, K. (2015*b*). *J. Electromagn. Waves Appl.* **29**, 132–142.
Zhukovsky, K. (2015*c*). *Opt. Commun.* **353**, 35–41.
Zhukovsky, K. (2016*a*). *Laser Part. Beams*, **34**, 447.
Zhukovsky, K. (2016*b*). *Nucl. Instrum. Methods Phys. Res. B*, **369**, 9–14.
Zhukovsky, K. (2017*a*). *Europhys. Lett.* **119**, 34002.
Zhukovsky, K. (2017*b*). *J. Phys. D Appl. Phys.* **50**, 505601.
Zhukovsky, K. (2017*c*). *J. Appl. Phys.* **122**, 233103.
Zhukovsky, K. V. (2018*a*). *Russ. Phys. J.* **60**, 1630–1637.
Zhukovsky, K. V. (2018*b*). *Russ. Phys. J.* **61**, 278–286.
Zhukovsky, K. (2018*c*). *Opt. Commun.* **418**, 57–64.
Zhukovsky, K. & Potapov, I. (2017). *Laser Part. Beams*, **35**, 326.